Applied Geochemistry 132 (2021) 105068

Contents lists available at ScienceDirect

Applied Geochemistry

journal homepage: www.elsevier.com/locate/apgeochem

Trace element and Pb and Sr isotope investigation of tooth enamel from archaeological remains at El-Kurru, Sudan: Evaluating the role of groundwater-related diagenetic alteration

Antonio Simonetti [a,*], Michele R. Buzon [b], Loretta Corcoran [a], Abagail M. Breidenstein [c], Geoff Emberling [d]

[a] Department of Civil and Environmental Engineering and Earth Sciences, University of Notre Dame, Notre Dame, IN, 46556, USA
[b] Department of Anthropology, Purdue University, West Lafayette, IN, 47907, USA
[c] Institut für Evolutionäre Medizin, Universität Zürich, Winterthurerstrasse 190, 8057, Zürich, Switzerland
[d] Kelsey Museum of Archaeology, University of Michigan, 434 South State Street, Ann Arbor, MI, 48109-1390, USA

ARTICLE INFO

Editorial handling by Dr Romain Millot

Keywords:
Tooth enamel
Pb and Sr isotope Ratios
El-kurru
ICP-MS
Groundwater alteration
Provenance

ABSTRACT

This study reports new trace element and Pb and Sr isotope compositions of tooth enamel from archaeological remains at a Medieval (Christian) cemetery located adjacent to the Kushite royal cemetery of El-Kurru, Sudan. The archaeological site of El-Kurru is located along the Nile River on the southern edge of the Nubian Plateau; the bedrock geology consists of Neoproterozoic crystalline basement and is overlain by fluvial sandstones and mudstones of Cretaceous age. El-Kurru is situated between two well-developed drainage basins, and in the past has been subjected to periodic (wadi-related) flooding as a result of intense local precipitation events. Enamel samples were taken from 18 individuals of varying ages and both sexes. Trace element abundances for a significant number of samples record elevated concentrations relative to modern ("in-vivo") enamel, including Pb and U; however, the abundances for both elements do not correlate significantly with the contents of the remaining trace elements (Ba, Fe, Mg, Mn, Nd, Sr) investigated here. The calculated enrichment factors for all trace elements studied here relative to average crustal values are not consistent with exposure to Pb ores for human purposes, which is corroborated by the Pb isotope results. The Sr isotope compositions define 2 main groups that yield $^{87}Sr/^{86}Sr$ ratios that are either higher or lower than 0.7072 with similar Sr abundances (range between ~100 and ~400 ppm). The Pb isotope compositions are extremely variable and correlate well with their corresponding U/Pb ratios; the former overlap Pb isotope ratios for proximal Neoproterozoic rocks belonging to the Saharan Metacraton and Arabian Nubian Shield tectonic provinces. The combined trace element abundances and Sr and Pb isotope compositions for the enamel samples located within the Christian cemetery at El-Kurru are best interpreted to record interaction with groundwater that occurred post-mortem during flooding events. As reported in previous anthropological studies of a similar nature, the Pb isotope results reported here are particularly sensitive to monitoring post mortem diagenetic alteration given their extremely low abundances in non-altered tooth enamel. In contrast, the $^{87}Sr/^{86}Sr$ ratios have been minimally perturbed by post mortem alteration, and therefore most likely represent individuals with distinct Sr isotopic signatures inherited from different geographic regions.

1. Introduction

1.1. $^{87}Sr/^{86}Sr$ ratios as provenance indicator and evaluating post mortem diagenesis in human tooth enamel

The use of strontium isotope ($^{87}Sr/^{86}Sr$) compositions has made an important contribution to understanding the provenance of materials in archaeology and interactions and migrations of ancient civilizations throughout the globe; such examples include Roman mobility in Europe (e.g., Schweissing and Grupe, 2003; Evans et al., 2006; Chenery et al., 2010) and the movements of the Wari, Inca, and Tiwanaku in South America (e.g., Knudson, 2008; Andrushko et al., 2009; Slovak et al.,

* Corresponding author.
E-mail address: simonetti.3@nd.edu (A. Simonetti).

https://doi.org/10.1016/j.apgeochem.2021.105068
Received 1 March 2021; Received in revised form 25 July 2021; Accepted 26 July 2021
Available online 30 July 2021

2009; Turner et al., 2009; Buzon et al., 2012). On Earth, the $^{87}Sr/^{86}Sr$ ratios of biological and geological materials vary as a function of the geological provinces, which are dependent on their age, and mineralogical make-up. Areas that are characterized by older bedrock with a higher proportion of minerals containing high Rb/Sr, such as micas (e.g., biotite, muscovite, alkali feldspar), will yield higher $^{87}Sr/^{86}Sr$ ratios compared to regions that contain younger rocks with lower Rb/Sr ratios. The reason being that the parent nuclide, ^{87}Rb, decays to the stable daughter isotope, ^{87}Sr, via beta decay (half-life of ~50 billion years). The $^{87}Sr/^{86}Sr$ ratios are then transferred into the hydrosphere and ecosphere through weathering. Animals record the $^{87}Sr/^{86}Sr$ compositions from their environment and diet and this signature is subsequently incorporated into their organic and skeletal tissues. Organic tissues that grow continuously, such as hair, teeth, bones, and tusks, may record temporal variations in the $^{87}Sr/^{86}Sr$ ratios, which can then be used to decipher migration patterns of individuals or groups from ancient civilizations. For example, Buzon et al. (2016) have effectively used the Sr isotope compositions of dental remains and faunal samples from archaeological sites of interest in Egypt's Nile Valley to distinguish between local (autochthonous) and non-local (allochthonous) populations. Of importance and as outlined in Bataille et al. (2018), $^{87}Sr/^{86}Sr$ ratios display a high resolution but predictable scalar spatial pattern that follow geological regimes and limited temporal variability. Therefore, spatiotemporal patterns of $^{87}Sr/^{86}Sr$ ratios in the geosphere, ecosphere and hydrosphere may provide precise and unique geolocation potential for provenance studies.

Caution must be exerted, however, when employing the Sr isotope compositions for the purposes of provenance determination as diagenetic modification by cumulative physical, chemical and/or biological alteration can perturb the original Sr isotopic signatures incorporated within ancient skeletal remains (e.g., Retzmann et al., 2019). Subsequent burial, Sr from the soil and/or groundwater of the entombment environment may accumulate in teeth. The predominant hydroxyapatite lattice of the latter may recrystallize and even form secondary minerals (e.g., brushite ($CaHPO_4{\cdot}2H_2O$) or carbonate ($CaCO_3$)) in micro-cracks, pores and vacancies (Nelson et al., 1986; Kohn et al., 1999; Nielsen--Marsh and Hedges, 2000; Prohaska et al., 2002; Hoppe et al., 2003), which may then alter the original, biogenic Sr isotope signature/fingerprint of the sample. In arid environments such as the Nile River valley, crystallization of secondary phases is the predominant process of diagenesis rather than bacterial alteration (Maurer et al., 2014; Dudás et al., 2016). Thus, several chemical indices are reported in order to evaluate the potential diagenetic alteration in studies of large populations for provenance identification. For example, elevated (>250 ppm) and depleted (<100 ppm) Sr contents in human enamel have been considered as indications of diagenetic changes (e.g., Dudás et al., 2016), which is also a function of the repository conditions (e.g., Sponheimer and Lee-Thorp, 2006). However, on the basis of Sr abundances (yielded a median value of 84 ppm) in fossilized human tooth enamel from 74 archaeological sites in Britain, the study by Evans et al. (2012) indicates these may reflect both diet and climate. Additionally, previous investigations of human and animal skeletal remains have shown that other indicators of diagenetic alteration include Ca/P (mass fraction) ratios above the theoretical value (2.16) of biogenic hydroxyapatite (Sillen, 1986), the presence of increased contents of elements, such as Al, Si, Ba, V, Fe and Mn, and/or the presence of elevated contents of ultra-trace elements (mainly REEs (rare earth elements), Y, Hf, Th, U; in vivo < 1 ppm; e.g., Kohn et al., 1999; Trueman et al., 2008; Koenig et al., 2009; Benson et al., 2013; Kohn and Moses, 2013; Willmes et al., 2016; Kamenov et al., 2018; Retzmann et al., 2019). Specifically, Kamenov et al. (2018) developed the maximum threshold concentrations (MTC) index as a means to evaluate post mortem addition of elements into preserved tooth enamel; MTC is calculated (in ppm) by taking the maximum concentration of an element established in pristine (non-altered) modern human tooth enamel and adding 2 times its documented standard deviation (STDEV). Thus, calculated C/MTC values of >1 when comparing elemental abundances for fossilized samples (C) to corresponding MTC values indicate post mortem addition (Kamenov et al., 2018).

Recently, Retzmann et al. (2019) developed a novel method for evaluating the degree of diagenetic alteration based on the comparison of the Sr abundances and isotope compositions of enamel and corresponding dentine; the latter exhibits a higher porosity, smaller crystallites, and a much higher organic content (~30%) relative to enamel and is therefore more susceptible to diagenetic alteration. However, the general consensus is that tooth enamel is not significantly affected by diagenesis due to its compact structure with very little pore space and a minor amount of organic content (~2%). Hence, tooth enamel is expected to preserve its original, biogenic Sr isotopic value and represents reliable sample material for investigating mobility and population migration studies (e.g., Kyle, 1986; Lee-Thorp and Sponheimer, 2003; Bentley, 2006; Buzon et al., 2007; Buzon and Simonetti, 2013; Montgomery, 2010; Slovak and Paytan, 2012; Szostek et al., 2015: Buzon et al., 2016; Schrader et al., 2019).

The comparative method outlined by Retzmann et al. (2019) obviously necessitates the analysis of both enamel and corresponding dentine (or bone) from the same individual in order to assess the degree of post-deposition diagenetic alteration. However, this approach may not always be feasible due to sampling issues. In this study, we propose an alternative approach which involves investigating the lead (Pb) isotope signatures in conjunction with the corresponding Sr isotope and trace elemental compositions of tooth enamel.

1.2. Pb isotopes as an environmental tracer

The lead and strontium isotopic compositions of an individual's hard tissues (tooth, bone) will reflect their diet (Ericson, 1985). Both elements may readily substitute for calcium in the hydroxyapatite matrix of teeth and bone (Nelson et al., 1986; Simons, 1986; Bercovitz and Laufer, 1990; Bowen, 2001; Simpson et al., 2021). Tooth enamel of permanent adult teeth forms during early childhood (typically during first 12 years of life) and is considered a dead tissue because it is not penetrated by any organic structures (Steele and Bramblett, 1988). Therefore, tooth enamel will reflect the isotope compositions of the (geologic) environment in which a person lived while the tooth was forming. This consists primarily of the bedrock geology associated with exposed land surfaces (top veneer) on Earth, which is the continental crust.

The continental crust makes up only ~0.6% by mass of the silicate Earth, but it does contain a very large proportion (20–70%; Rudnick and Fountain, 1995) of incompatible elements; the latter are preferentially incorporated in Earth's crust and not the upper mantle due to incompatible size and/or charge in predominant mantle minerals, which include uranium (U) and lead (Pb). Lead has 4 isotopes: ^{204}Pb, ^{206}Pb, ^{207}Pb, and ^{208}Pb, and the latter three are the stable daughter products from the radiogenic decay of long-lived isotopes ^{238}U, ^{235}U, and ^{232}Th, respectively, in addition to their primordial abundances present at the time of solar system/Earth formation. In contrast, ^{204}Pb is the only non-radiogenic isotope of Pb, and its abundance is thus constant in nature. Therefore, the present-day Pb isotope composition of any geological sample is a function of its Pb isotope composition at the time of its formation, the U–Pb–Th ratios, and its age. Due to the large variations in the geochemical behavior of U, Th, and Pb, the Pb isotopic composition of rocks, minerals (e.g., galena – PbS), and ores display a significant natural variation, which can be used as an isotopic "fingerprint." As such, this fingerprint may be employed to link Pb ores and the industrial (anthropogenic) materials produced from them (Brill and Wampler, 1967; Iñañez et al., 2010; Sangster et al., 2000). Moreover, ancient civilizations have extracted Pb from ore deposits over thousands of years for a variety of purposes (metallurgical, medicinal, and industrial), hence, rendering Pb one of the most heavily utilized metals during human history. Previous investigations have demonstrated that reporting the Pb isotope compositions of archaeological materials, such as

kohls and glass (e.g., Shortland, 2006) and pottery glazes (e.g., Iñañez et al., 2010; Schurr et al., 2018), the mineral galena (PbS) (e.g., Shortland, 2006; Mirnejad et al., 2011, 2015), and ancient human and prehistoric animal teeth (e.g., Samuelsen and Potra, 2020) is effective for shedding light on transport and trade practices of metals and ores in ancient civilizations and source attribution purposes in crustal environments.

Numerous previous human epidemiological investigations indicate that Pb abundances in hard tissues such as bone and tooth typically represent a longer-term indicator of several years (e.g., Gulson, 1996; Johnston et al., 2019). Unlike the relatively high concentrations of Sr (hundreds of ppm) in tooth enamel and dentine, the range of Pb abundances in teeth is in general an order of magnitude lower (i.e., ~1–10s of ppm; Gulson, 1996; Purchase and Fergusson, 1986; Wychowanski and Malkiewicz, 2017; Johnston et al., 2019). Higher Pb contents in hard tissue may be indicative of exposure to elevated levels of this metal in the environment, whether it is of natural (geogenic) or anthropogenic (human activity-related) origin. However, it is only through the combined investigation of both the Pb abundances and their corresponding isotopic compositions can an accurate assessment or interpretation be rendered in relation to source attribution purposes.

In this study, the Sr and Pb isotope compositions and trace element abundances of tooth enamel are reported for human remains buried at El-Kurru, Sudan (Fig. 1; Emberling et al., 2013; Emberling et al., 2015; Dann et al., 2016). The burials were part of a Medieval (Christian) walled settlement (ca. 600–1400 CE) located on the edge of the Nile floodplain. The Kushite royal cemetery for which El-Kurru is known is located some 400 m to the northwest, on the edge of the desert plateau. This site was chosen for investigation because of the overall poor preservation of the skeletal remains and its unique location in relation to several well-developed drainage systems along the Nile River at El-Kurru. Evidences obtained from taphonomy and observed diagenetic changes in skeletal remains indicate that the site has experienced periodic flooding, and therefore, these events may have impacted the isotopic and trace elemental abundances preserved in tooth enamel for individuals at this site.

2. Local geology, hydrology and samples

2.1. Local geology

El-Kurru is located along the Nile River on the southern edge of the Nubian Plateau, which consists of a Neoproterozoic bedrock core that is overlain by horizontal sedimentary rocks (Fig. 1; Dann et al., 2016). The site of El-Kurru is situated proximal to the suture between the Arabian Nubian Shield (ANS) and Saharan Metacraton (SMC) in the Bayuda Desert (Fig. 1). The crystalline basement rocks within the ANS are interpreted as juvenile (newly formed) Neoproterozoic crust and represent dismembered ophiolite (e.g., Abdel-Rahman, 1993; Abdelsalam et al., 1998), whereas those from the SMC represent older cratonic crust that was deformed during the Neoproterozoic (between ~1000 and ~550 Ma), and consist of polymetamorphic amphibolite from magmatic arc environments (e.g., Küster and Liégeois, 2001). The bedrock at the site consists of overlying fluvial sandstones and siltstones of probable Cretaceous age (Geological Research Authority of the Sudan, 1988; Geologic Map of Sudan). At El-Kurru, the Nile has carved into the Neoproterozoic crystalline basement and there is localized floodplain development (Dann et al., 2016).

Within the royal cemetery, the rock exposures in the staircases and chambers consist of a sequence of Cretaceous sandstones, siltstones, and mudstones >5 m thick (Dann et al., 2016). The lowest unit comprises alternating layers of sandstone, siltstone, and mudstone (with thicknesses ~1.5–~2 m) that represent either channel (sandstone) or floodplain deposits of ancient rivers (Dann et al., 2016). Moreover, the top of the lowermost sandstone unit is overlain by a paleosol, which consists of thin layers of hard, Fe-cemented, typically fine-grained sediments that represent buried soil horizons; therefore, these may be referred to as ferricretes (Dann et al., 2016). These Cretaceous-aged rock units are overlain unconformably by a thin layer of sandy Quaternary gravels.

2.2. Hydrology

The site of El-Kurru is situated between two large, well-developed drainage basins, but the area itself is drained by a smaller and less developed drainage system (Dann et al., 2016). Large-scale flooding events along the Nile are related primarily to the humid climate present at the southern headwaters' region, and three such episodes were

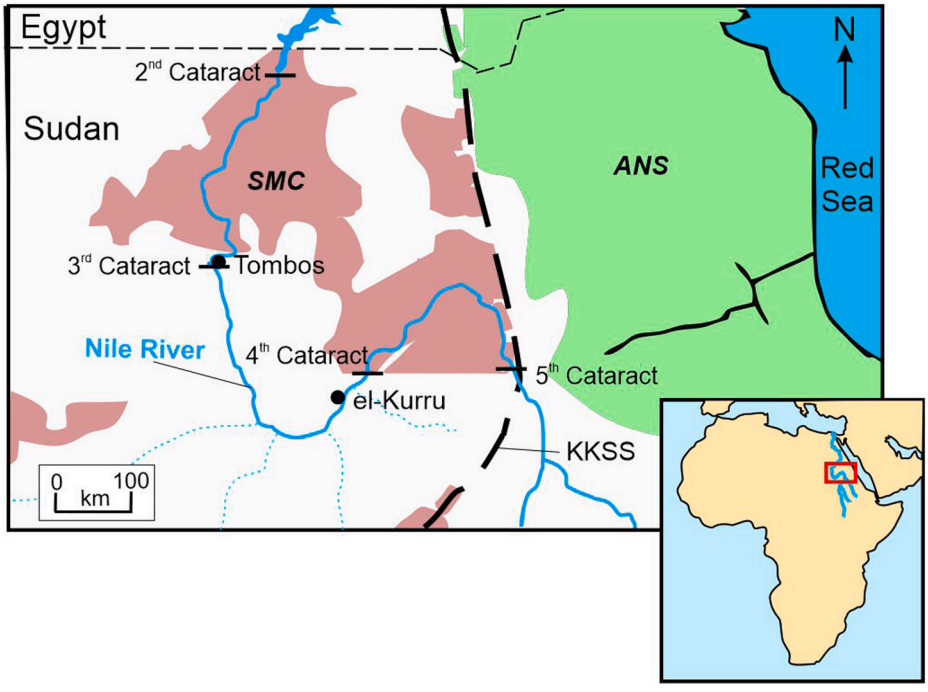

Fig. 1. Inset shows location of study area (red rectangle) within continental Africa. Main diagram is a map illustrating the regional geology of northeastern Sudan, which outlines the cratonic crust with Neoproterozoic deformation referred to as the Saharan Metacraton (SMC, red areas), and Neoproterozoic juvenile crust of the Arabian Nubian Shield (ANS, green area). Also shown are the locations of burial site at El-Kurru (present study) and the archaeological site of Tombos, both along the Nile River. Dashed line labeled KKSS = Keraf Kabus Sekerr Suture zone between ANS and SMC crustal provinces. Map is modified after Evuk et al. (2017). (For interpretation of the references to color in this figure legend, the reader is referred to the Web version of this article.)

recorded in 1946, 1988, and 1994 (Dann et al., 2016). In contrast, the flooding of the wadi draining the site at El-Kurru is attributed to intense local precipitation events, which in a typical year can occur two to three times and results in strong, channelized, knee-deep (at best) flow for about 1 h (Dann et al., 2016). Recent excavations revealed that the late mortuary temple located next to the wadi was flooded and ~500 mm of sediment was deposited (Emberling et al., 2015); it is postulated that overland flow from areas surrounding the temple likely contributed to this depositional event. Taphonomy and diagenetic changes have most likely been impacted by water damage that has affected the cemetery for centuries. This cemetery was located at an opening fan of a seasonal wadi and close to the banks of the Nile; it is in close proximity to flooded irrigated palm groves and other agricultural land still in use. Therefore, it is very likely that the cemetery and skeletons have incurred water damage over the centuries.

2.3. Samples

Excavations in 2014–2016 uncovered 27 individuals in the Christian cemetery, of which 18 were examined in this study. A Christian date for these graves was suggested based on the scarcity of grave goods as well as approximate west-east orientation (relative to the Nile River) and treatment of the bodies; heads of all individuals were oriented cardinally in the northwestern direction, their feet in the southeast, with either their arms or ankles crossed (Dann et al., 2016; Welsby, 2002). Radiocarbon dating of the El-Kurru skeletons has proven difficult due to the poor preservation of collagen. Thus, date estimations are based on the ^{14}C dating of the fortification wall, the mortuary archaeology, and stratigraphy of the skeletal remains. Organics from the wall were ^{14}C dated to *ca.* 600–1000 CE (Dann et al., 2016). Additionally, pottery sherds and decoration motifs date the fills to Classic (*ca.* 800–1100 CE) or Late Christian (*ca.* 1100–1450 CE) and one Islamic glass bead was found in an unusual context, but still indicate these burials date at *ca.* 1450 CE. Lastly, the stratigraphy of the cemetery indicates that these burials represent the last phase of occupation in this area. Table 1 lists the approximate ages, sex and burial depths associated with the type of tooth enamel sample investigated in this study. Of note, not all 27 individuals uncovered were examined/sampled due to either extremely poor preservation of the tissue leading to not enough material to sample, teeth not recovered from an individual (e.g., adult KU216 was edentulous), and/or that some subadults did not have enough mineralized material for testing. For this study, sample selection included intact teeth whenever possible and those with enamel that was macroscopically in good condition. Generally, all tooth preservation was graded as good or satisfactory (Enamel Preservation Classification Score of between 3 and 4; Montgomery, 2002). Most crowns were fully intact (i.e., not too fragmented) with some thin cracks, some superficial soil concretions or evidence of plant abrasion, and in some cases separation from the underlaying dentine. Despite the presence of such damages and moderate to severe occlusal attrition in almost all adult teeth, the enamel of the selected teeth was generally hard, glossy, and milky-white with only some small areas of discoloration. Some teeth were previously harvested of dentine for ancient DNA analysis in a clean lab. When sampled, the crown was removed from the root with a thin sectioning blade for access to the inner dentine for sampling, leaving the crown enamel intact for further processing. Enamel samples were mechanically cleaned and abraded before chemical purification to reduce post-depositional contamination.

Table 1
Information for tooth enamel samples from El-Kurru investigated here.

Sample #	Tooth	Sex Estimation	Age Estimation (in years)	Median Burial Elevation (meters)
KUR-01	PM	Probable Female	Adolescent (15± 3)	248.74
KUR-02	M1	Indeterminate	Child (3± 1)	249.35
KUR-03	PM^2	Male	Young Adult (20–35)	248.89
KUR-04	PM_2	Indeterminate	Adolescent (15± 3)	248.80
KUR-05	PM	Indeterminate	Middle Adult (36–50)	248.82
KUR-06	PM_1	Indeterminate	Child (7–9)	249.02
KUR-07	PM	Probable Female	Older Adult (50+)	249.06
KUR-08	PM	Male	Young Adult (20–35)	249.10
KUR-09	PM^1	Female	Young Adult (20–35)	248.85
KUR-10	PM_1	Indeterminate	Older Adult (50+)	n.d.
KUR-11	PM_2	Probable Male	Older Adult (50+)	248.85
KUR-12	dm_1	Indeterminate	Child (4.5)	249.39
KUR-13	M^1	Indeterminate	Child (7.5)	249.11
KUR-14	M_3	Probable Female	Middle Adult (36–50)	248.84
KUR-15	PM_x	Male	Older Adult (50+)	249.29
KUR-16	dm_1	Indeterminate	Child (3.5)	249.40
KUR-17	PM_1	Indeterminate	Adolescent (17.5)	248.93
KUR-18	dm_1	Indeterminate	Child (5.5+)	249.31

M = unspecified molar; PM = premolar; M_3 = third molar; dm_1 = first deciduous molar; PM_1 = first premolar; PM_2 = second premolar. n.d. = not determined.

3. Analytical methods

3.1. Trace element geochemistry

Samples of tooth enamel were processed in two steps. In the first step, between ~70 and ~300 mg of enamel was placed in a 15 mL Savillex® Teflon beaker and ~4 mL of concentrated 16N, double-distilled (DD) HNO_3 was added, followed by heating on a hotplate at 110 °C for 24h. After the heating, samples were removed from the hotplate and cooled for 1 h. After rinsing the sample residues adhered to the sides of the beakers with 18 MΩ cm^{-2} water, samples were placed back on the hotplate to achieve complete dryness. In the second cycle, all conditions were kept the same, except the amount of 16N DD HNO_3 acid was decreased from 4 to 1 mL. After the last drying step, 5 mL of 16N DD HNO_3 acid was added into the beaker and the solution diluted with 18 MΩ cm^{-2} water until a final total volume of ~100 mL was achieved. Appropriate sample volume aliquots for trace element and Sr and Pb isotope analyses were taken from the 100 mL solution. The concentrations of the trace elements (Table 2) were determined by a standard/spike addition method (Jenner et al., 1990), which includes correction for matrix effects and instrumental drift.

The trace element abundances (Table 2) for all samples were determined using an Attom (Nu Instruments Ltd., Wales, UK) high resolution inductively coupled plasma mass spectrometer (HR-ICP-MS) in medium mass resolution mode ($M/\triangle M \approx 3000$). Samples were processed using a wet plasma, solution mode introduction system that consists of a cyclonic spray chamber (housed within a Peltier cooling device @7 °C) and Meinhard nebulizer (aspiration rate of 0.1 mL/min). Before each analytical session, the Attom instrument was tuned and calibrated using a multi-elemental (Li, B, Na, Si, Sc, Co, Ga, Y, Rh, In, Ba, Lu, Tl, U) 1 ppb (ng g-1) standard solution.

Enrichment factors (EF) have been calculated for each sample for several of the trace elements (e.g., Mn, Sr, Pb, U) with elevated contents (relative to in vivo, modern day human enamel), and these are listed in Table 2. The EFs evaluate the relative contribution from either natural (i.e., soil, bedrock) vs. anthropogenic sources (e.g., ores used for kohl or ceramic glaze production) of a given element in the tooth enamel. $EF_{ELEMENT}$ is defined as the concentration ratio of a given element to that of Mg in this case (or any other element thought to be derived exclusively from a crustal source, such as Si, Al) normalized to the same concentration ratio characteristic of the upper continental crust (e.g.,

Table 2
Trace element concentrations (ppm) and enrichments factors for Pb, U, Sr, and Mn for samples of tooth enamel from El-Kurru in this study.

Sample	Mg	Mn	Fe	Sr	Ba	Nd	Pb	U	U/Pb	EF_{Pb}	EF_{U}	EF_{Sr}	EF_{Mn}
KUR-1	2276	3.53	286	188	10	0.07	0.16	0.18	1.12	0.06	0.45	3.85	0.03
KUR-2	2148	21.52	436	245	36	0.19	1.28	0.30	0.23	0.52	0.77	5.33	0.19
KUR-3	2215	34.34	400	343	80	0.38	9.58	1.52	0.16	3.80	3.79	7.24	0.30
KUR-4	2289	2.52	302	172	6	0.13	0.11	0.07	0.58	0.04	0.16	3.51	0.02
KUR-5	973	11.76	141	106	19	0.06	0.23	0.20	0.86	0.21	1.12	5.12	0.23
KUR-6	2627	13.02	325	221	16	0.09	0.71	0.16	0.23	0.24	0.34	3.93	0.10
KUR-7	2942	13.85	565	398	52	0.35	0.85	0.21	0.25	0.25	0.40	6.33	0.09
KUR-8	2513	20.19	352	188	19	1.15	0.33	0.08	0.24	0.11	0.17	3.50	0.16
KUR-9	2605	7.09	338	256	36	0.18	0.43	0.42	0.97	0.15	0.89	4.59	0.05
KUR-10	3181	8.35	391	236	27	0.28	0.97	0.32	0.33	0.27	0.55	3.47	0.05
KUR-11	2629	41.77	509	225	15	0.50	61.95	0.34	0.01	20.7	0.71	4.00	0.31
KUR-12	2675	29.20	368	291	81	0.38	22.47	1.30	0.06	7.4	2.69	5.08	0.21
KUR-13	2507	9.09	317	115	10	0.90	3.17	0.12	0.04	1.11	0.26	2.15	0.07
KUR-14	2485	17.18	369	425	73	0.22	0.63	0.47	0.75	0.22	1.05	7.99	0.13
KUR-15	2695	41.23	393	286	25	0.76	0.29	0.35	1.20	0.10	0.72	4.96	0.30
KUR-16	2537	66.23	440	290	82	0.32	2.89	1.40	0.48	1.00	3.06	5.35	0.50
KUR-17	2621	9.26	278	181	14	0.10	2.60	0.11	0.04	0.87	0.24	3.22	0.07
KUR-18	2256	23.76	322	169	33	0.31	7.73	0.71	0.09	3.01	1.75	3.51	0.20

The 2σ level relative standard deviation (RSD% = standard deviation/average concentration x 2 x 100) is a function of absolute elemental concentration, and thus varies between ~2.5 and ~6.0% for the more abundant elements (Mg, Mn, Fe, Sr, Ba) and between ~15 and ~46% for Nd, Pb, and U (≪ 1 ppm).

Rudnick and Gao, 2014). In this study, Mg was chosen for this normalization since it is typically an element of natural origin and may substitute for Ca in tooth enamel (LeGeros, 1991); in addition, Mg contents do not correlate with any of the other trace elements investigated here (not shown). For example, the enrichment factor for Pb is thus: $(EF)_{Pb} = [Pb/Mg]_{sample}/[Pb/Mg]_{crust}$. However, given the large natural variations in the composition of crustal materials exposed to surface erosion and the diversity of biogeochemical processes affecting soil development at a global scale, enrichment factors within ±10 times the mean crustal abundances (i.e., EF values between 0.1 and 10) most likely indicate elements derived from continental crust (Duce et al., 1976). Conversely, any $(EF)_{element}$ >10 suggests contributions from other sources, such as human activities.

3.2. Sr isotope compositions

Separation and purification of Sr for subsequent Sr isotope analysis involved ion exchange chromatography, which employed columns containing 1.7 mL of 200–400 mesh AG50W-X8 resin. Sample aliquots (containing ~300 ng total Sr) in 0.25 mL of 2.5N DD HCl were loaded onto the resin beds; this was followed by several additional wash steps totaling ~15 mL of 2.5N DD HCl acid, and the Sr was subsequently eluted with 4 mL of 2.5N DD HCl. After the ion exchange chemistry, Sr-bearing aliquots were dried, dissolved in 2% HNO_3 solution (~2 mL) and aspirated into the ICP torch using a desolvating nebulizing system (DSN-100 from Nu Instruments Ltd.). Strontium isotope measurements were conducted using a NuPlasma II MC-ICP-MS (multi-collector inductively coupled plasma mass spectrometer; Nu Instruments Ltd.) instrument according to the protocol outlined in Balboni et al. (2016). Strontium isotope data was acquired in static, multi-collection mode using 5 Faraday collectors for a total of 400 s, consisting of 40 scans of 10 s integrations. The analytical protocol's accuracy and reproducibility were verified by analyzing the NIST SRM 987 strontium isotope standard during two analytical sessions, which yielded an average value of 0.710235 ± 0.000044 (2σ; n = 4), in agreement with the certified value of 0.71025 (Faure and Mensing, 2005).

3.3. Pb isotope compositions

The Pb separation method is adapted from Manhes et al. (1980) and a brief summary is provided here (after Koeman et al., 2015). The Pb ion exchange micro-columns consist of approximately 20 μL of clean AG1-X8 resin (75–150 mesh) placed into a polypropylene tube combined with a polystyrene frit. The resin volume is cleaned using 0.15 mL of ultrapure (18 MΩ cm^{-2}) H_2O, and further conditioned with 0.15 mL of 0.8 N DD HBr. The sample solution was loaded with 0.6 mL of 0.8 N DD HBr, washed twice with 0.15 mL of 0.8 N DD HBr, and last eluted with 0.7 mL of 6 N DD HCl acid. After the eluted Pb is dried down, the ion exchange procedure is repeated with fresh resin in order to further purify the Pb aliquot. Following the last elution procedure, the Pb aliquot is dried down and dissolved again in 2% HNO_3 for solution mode MC-ICP-MS analysis.

Pb isotope compositions of the sample solutions were determined using the same procedure outlined in Simonetti et al. (2004). After the purification steps, the aliquot of Pb was spiked with a NIST SRM 997 Thallium standard solution (2.5 ppb). Seven Faraday cups on the Nu Plasma II MC-ICPMS instrument were employed to simultaneously measure the Pb and Tl isotopes and ^{202}Hg. The instrumental mass bias (exponential law; $^{205}Tl/^{203}Tl = 2.3887$) is determined by measuring the $^{205}Tl/^{203}Tl$, and ^{202}Hg is monitored to correct for the interference of ^{204}Hg on ^{204}Pb. Prior to the aspiration of the samples into the plasma, ion signals for the gas and acid blanks ("on-peak-zeros") were recorded for 30 s to determine baseline values. For each analysis, data acquisition involved 2 blocks of 25 scans (each scan has a 10 s integration time). A 25-ppb solution of the NIST SRM 981 Pb standard (spiked with 6 ppb NIST SRM 997 Tl standard) was measured periodically during the analytical session in order to validate the Pb isotope results. The average Pb isotope ratios and associated 2σ standard deviations obtained on 3 measurements of the NIST SRM 981 Pb isotope standard for two analytical sessions are as follows: $^{206}Pb/^{204}Pb = 16.939 \pm 0.007$, $^{207}Pb/^{204}Pb = 15.493 \pm 0.007$, $^{208}Pb/^{204}Pb = 36.699 \pm 0.008$, $^{208}Pb/^{206}Pb = 2.1666 \pm 0.0002$, and $^{207}Pb/^{206}Pb = 0.91464 \pm 0.00004$, which overlap with certified values for this standard (Baker et al., 2004).

4. Results

Tables 2 and 3 list the trace element abundances and Sr and Pb isotope compositions for the 18 samples of tooth enamel from El-Kurru investigated here, respectively; these data are also illustrated in Figs. 2–8. The Sr abundances for the tooth enamel vary between 106 and 425 ppm (Table 2; Fig. 2), and a majority fall within the range considered to represent diagenetically unaltered material (between 100 and 250 ppm; Dudás et al., 2016). Six samples (KUR-3, -7, -12, −14, −15, −16) contain elevated Sr abundances (>250 ppm and up to 425 ppm; Table 2). Fig. 2 plots the concentrations of Sr versus those for several trace elements, Mg, Ba, and U; Mg abundances do not exhibit any correlation with Sr contents (Fig. 2a), whereas Ba and U show a fairly good positive correlation (R^2 correlation coefficient ≈ 0.74), respectively

Table 3
Sr and Pb isotope compositions for samples of tooth enamel from El-Kurru.

Sample #	$^{87}Sr/^{86}Sr$	$^{206}Pb/^{204}Pb$	$^{207}Pb/^{204}Pb$	$^{208}Pb/^{204}Pb$	$^{208}Pb/^{206}Pb$	$^{207}Pb/^{206}Pb$	$^{208}Pb/^{207}Pb$
KUR-1	0.70748(1)	23.081(21)	15.934(2)	38.609(4)	1.6728(16)	0.6904(6)	2.4230(6)
KUR-2	0.70772(2)	19.503(1)	15.741(1)	38.501(2)	1.9741(2)	0.8071(1)	2.4459(1)
KUR-3	0.70799(1)	18.308(1)	15.643(1)	38.384(2)	2.0965(1)	0.8544(1)	2.4537(1)
KUR-4	0.70694(1)	56.351(.98)	18.060(.87)	37.917(.5)	0.6826(.1)	0.3176(.04)	2.0995(.05)
KUR-5	0.70712(1)	19.799(1)	15.757(1)	38.503(1)	1.9448(1)	0.7958(1)	2.4436(1)
KUR-6	0.70668(2)	18.496(1)	15.672(1)	38.477(1)	2.0803(1)	0.8473(1)	2.4551(1)
KUR-7	0.70831(2)	19.056(3)	15.721(1)	38.479(1)	2.0192(4)	0.8250(2)	2.4476(2)
KUR-8	0.70812(1)	19.001(1)	15.693(1)	38.530(2)	2.0278(1)	0.8259(1)	2.4552(1)
KUR-9	0.70670(2)	19.748(2)	15.747(1)	38.516(2)	1.9504(2)	0.7974(1)	2.4460(1)
KUR-10	0.70696(1)	20.503(1)	15.806(1)	38.483(1)	1.8769(1)	0.7709(1)	2.4347(1)
KUR-11	0.70768(1)	18.715(1)	15.704(1)	38.481(2)	2.0561(1)	0.8391(1)	2.4504(1)
KUR-12	0.70772(1)	18.338(1)	15.688(1)	38.538(1)	2.1015(1)	0.8555(1)	2.4566(1)
KUR-13	0.70688(1)	18.812(1)	15.702(1)	38.460(1)	2.0444(1)	0.8347(1)	2.4493(1)
KUR-14	0.70678(1)	19.077(1)	15.715(1)	38.508(2)	2.0186(1)	0.8238(1)	2.4504(1)
KUR-15	0.70663(1)	22.464(15)	15.987(1)	38.531(3)	1.7150(12)	0.7116(4)	2.4102(4)
KUR-16	0.70678(1)	18.369(1)	15.692(1)	38.561(2)	2.0993(1)	0.8543(1)	2.4574(1)
KUR-17	0.70679(1)	18.511(1)	15.664(1)	38.412(2)	2.0751(1)	0.8462(1)	2.4522(1)
KUR-18	0.70677(1)	18.292(1)	15.676(1)	38.443(2)	2.1017(1)	0.8570(1)	2.4523(1)

Number in parenthesis represents uncertainty (2σ level) in the last digits reported except for sample Kur-4.

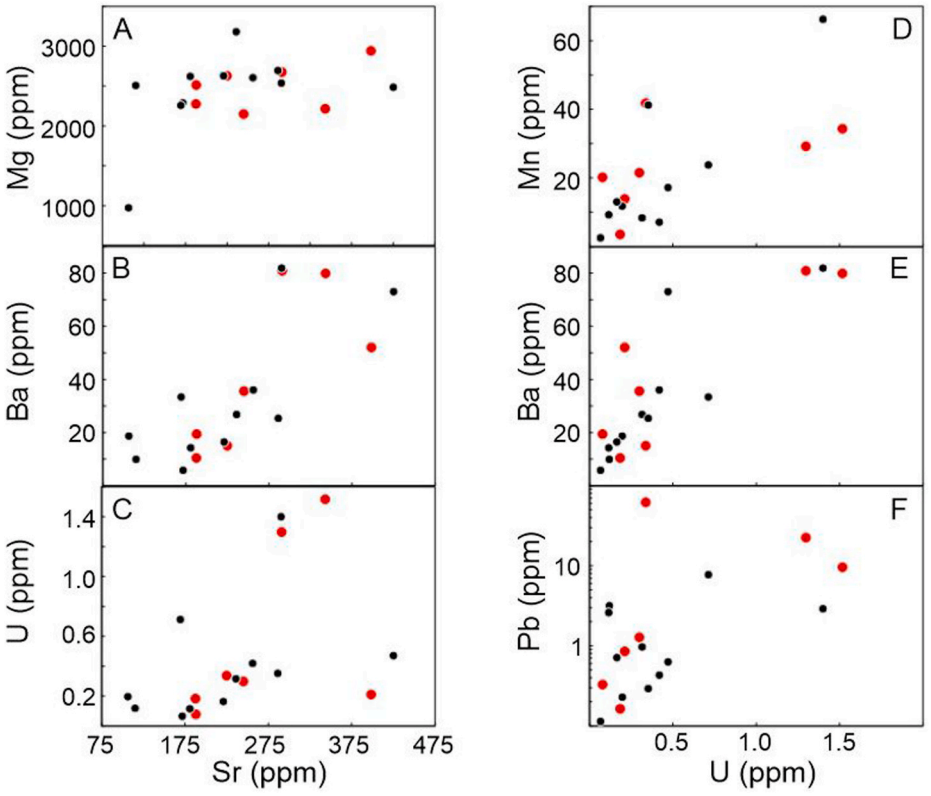

Fig. 2. Bivariate plots displaying the concentrations (all expressed in ppm) of Sr versus those for (A) Mg, (B) Ba, and (C) U, and U compared to those for (D) Mn, (E) Ba, and (F) Pb for samples of tooth enamel from El-Kurru examined in this study. Red and black solid circles represent samples of tooth enamel with high and low $^{87}Sr/^{86}Sr$ as defined in Fig. 4 and detailed in text. (For interpretation of the references to color in this figure legend, the reader is referred to the Web version of this article.)

(Fig. 2b and c). The contents of Mn and Pb versus those of U are also illustrated in Fig. 2d–f, and these in general all correlate positively. Of note, the contents of U, Nd, and Fe reported here for all samples exceed C/MTC normalized values > 1 (Fig. 3); a C/MTC value ≤ 1 is considered to be representative of non-altered samples and equivalent to modern-day tooth enamel (i.e., in vivo; Kamenov et al., 2018). In Fig. 3, the normalized C/MTC values for the remaining elements are all <1 with the exception of Mn and Ba, which fluctuate slightly on either side of unity. Overall, the C/MTC patterns shown in Fig. 3 are not consistent for all of the samples investigated. Lastly, the vast majority of the enrichment factors (EFs) listed for Mn, Pb, Sr, and U in Table 2 vary between 1 (or <1) and 10, with the exception of tooth enamel sample KUR-11 that records a EF_{Pb} of ~21.

The Sr isotope compositions for the KUR enamel samples investigated here define two groups relative to their corresponding Sr contents (Fig. 4; Table 2), and these overlap primarily the range of variable, present-day $^{87}Sr/^{86}Sr$ ratios for metamorphic rocks from the SMC (~0.7030–~0.7089) and not with the less radiogenic signatures (~0.7030–~0.7053) for the metamorphic rocks from the ANS tectonic province (Evuk et al., 2017).

As discussed earlier, assessing the Pb isotope compositions of geological, environmental, or industrial samples provide an effective means for provenance determination. Table 3 lists the Pb isotope compositions for the tooth enamel samples investigated here, and these are illustrated in Figs. 5–7. In Fig. 5, the Pb isotope data for the tooth enamel samples are compared to those for rocks belonging to both the

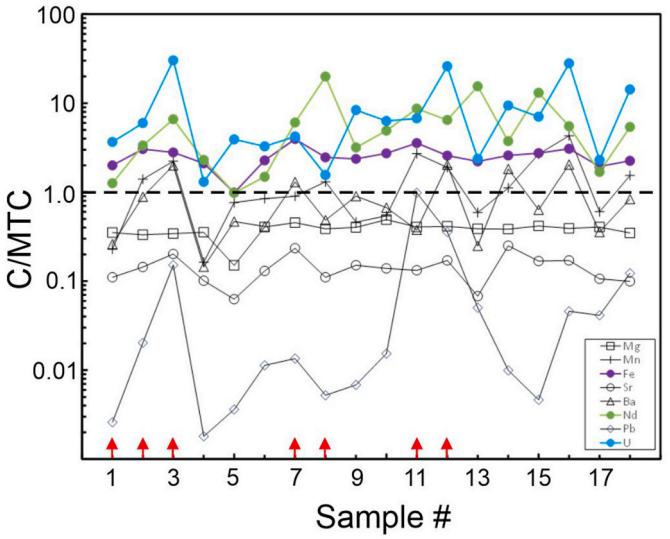

Fig. 3. Trace element abundances for El-Kurru human enamel samples investigated here (Table 2) normalized to those established by maximum threshold concentration (MTC) index after Kamenov et al. (2018). C/MTC = Concentration (C) of trace element (ppm) divided by corresponding MTC value. The red arrows indicate samples characterized by high $^{87}Sr/^{86}Sr$ ratios (Fig. 4). Dashed horizontal line at unity (C/MTC value = 1.0) separates elements/samples affected by post mortem diagenetic alteration (>1.0) versus non-altered (<1.0). (For interpretation of the references to color in this figure legend, the reader is referred to the Web version of this article.)

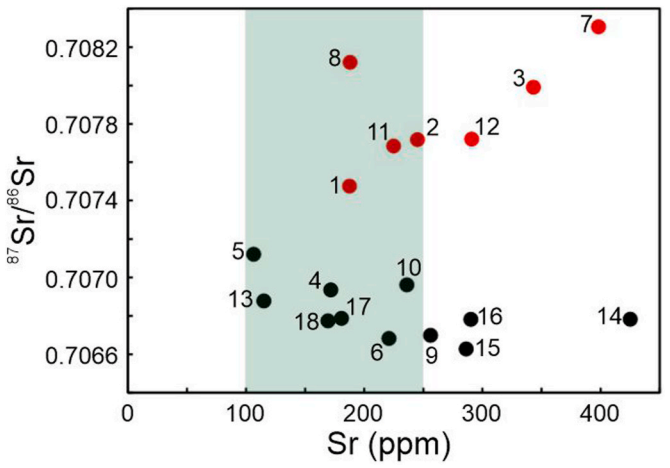

Fig. 4. Diagram illustrates the Sr contents (ppm) versus their corresponding Sr isotope compositions for the samples of tooth enamel from El-Kurru investigated here. The samples define two groups relative to their $^{87}Sr/^{86}Sr$ ratios, those with higher (red) compared to those with lower (black) signatures. The shaded region represents the range of Sr abundances considered to represent unaltered, pristine tooth enamel (100–250 ppm; Dudás et al., 2016). Numbers adjacent to data points refer to corresponding sample numbers (Tables 1–3). Associated uncertainties for both Sr contents and isotope compositions are within the size of the symbol. (For interpretation of the references to color in this figure legend, the reader is referred to the Web version of this article.)

neighboring SMC and ANS tectonic provinces (Evuk et al., 2017), which indicate a substantive degree of overlap, in particular with those from the SMC. In addition, Fig. 5 also contains the Stacey and Kramers (1975) evolution curve, which represents the time-integrated Pb isotope composition of average continental crust over the past 3.7 billion years. The Pb isotope compositions for the El-Kurru enamel samples mainly plot above and to the right of the Stacey and Kramers (1975) Pb evolution curve (S/K), and define well constrained linear arrays. In the

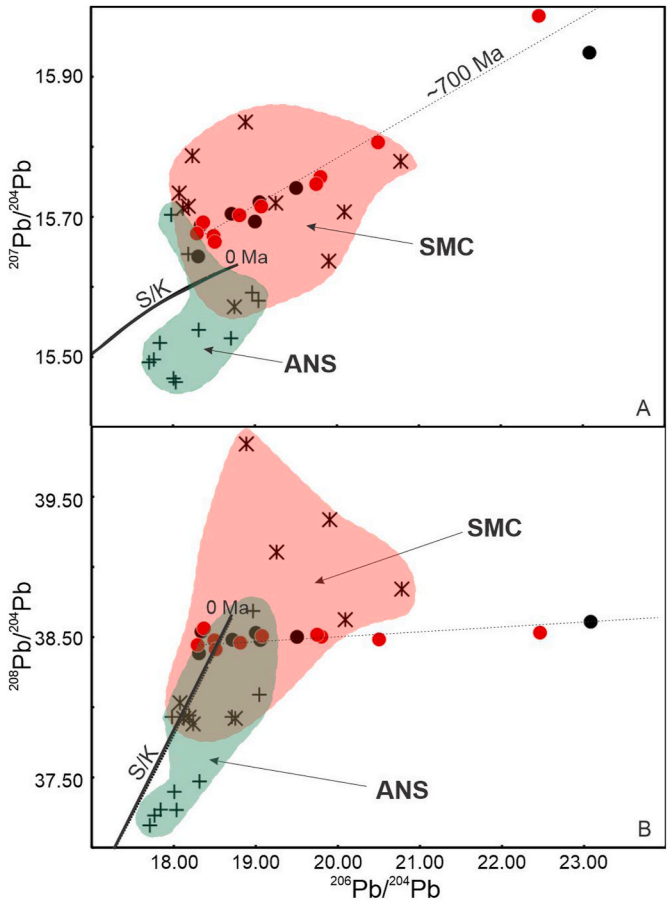

Fig. 5. Plots of $^{206}Pb/^{204}Pb$ versus (A) $^{207}Pb/^{204}Pb$ and (B) $^{208}Pb/^{204}Pb$ for samples of tooth enamel from El-Kurru examined here (with the exception of sample KUR-4 in order to maximize scaling). These are compared to Pb isotope compositions (from Evuk et al., 2017) for samples of juvenile Neoproterozoic crust from the neighboring Arabian Nubian Shield (+, green field) and the Neoproterozoic Saharan Metacraton (*, red field; areas shown in Fig. 1). Also shown is the Pb isotopic evolution curve for average continental crust (S/K; Stacey and Kramers, 1975). Red and black solid circles refer to group designation based on their corresponding Sr isotope compositions (Fig. 4). In (A) El-Kurru samples define a best-fit linear regression line with a slope that corresponds to a secondary isochron age of approximately 700 million years (Ma), which is similar to the age of the surrounding basement rocks of the ANS and SMC. Associated uncertainties are within the size of the symbol. (For interpretation of the references to color in this figure legend, the reader is referred to the Web version of this article.)

$^{206}Pb/^{204}Pb$ versus $^{207}Pb/^{204}Pb$ plot, the best-fit regression line defines a slope of 0.0629, which corresponds to a Neoproterozoic $^{207}Pb/^{206}Pb$ age of approximately 705 million years old; the latter corresponds to the age of the crystalline basement in the region (e.g., Evuk et al., 2017). Typically, any linear array on a Pb–Pb isotope plot is considered to represent either binary mixing between two distinct end-member components (i.e., resulting from open system behavior), or may simply reflect the addition of radiogenic Pb resulting from the decay of U over geologic time. Both of these hypotheses will be evaluated and discussed in the following section.

5. Discussion

Fig. 4 plots the Sr abundances versus their corresponding $^{87}Sr/^{86}Sr$ ratios for the tooth enamel samples from El-Kurru examined here. Hypothetically, enamel for individuals that lived or originated from the same geologic area and have not been affected by post mortem diagenesis should define a restricted field; in particular, the range in Sr

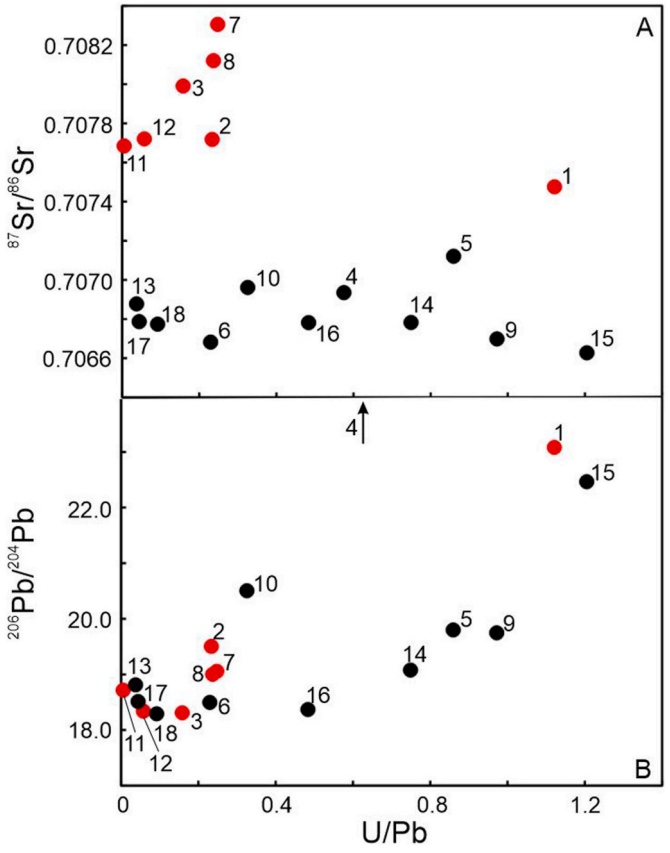

Fig. 6. Diagrams illustrate U/Pb ratios versus (A) $^{87}Sr/^{86}Sr$ and (B) $^{206}Pb/^{204}Pb$ for samples of tooth enamel from El-Kurru examined here. Red and black solid circles refer to group designation based on their corresponding Sr isotope compositions (Fig. 4) and numbers refer to sample numbers (Tables 1–3). The data point corresponding to sample KUR-4 is not shown for scaling purposes due to its extremely radiogenic Pb isotope composition ($^{206}Pb/^{204}Pb = 56.351$; Table 3). Associated uncertainties are within the size of the symbol. (For interpretation of the references to color in this figure legend, the reader is referred to the Web version of this article.)

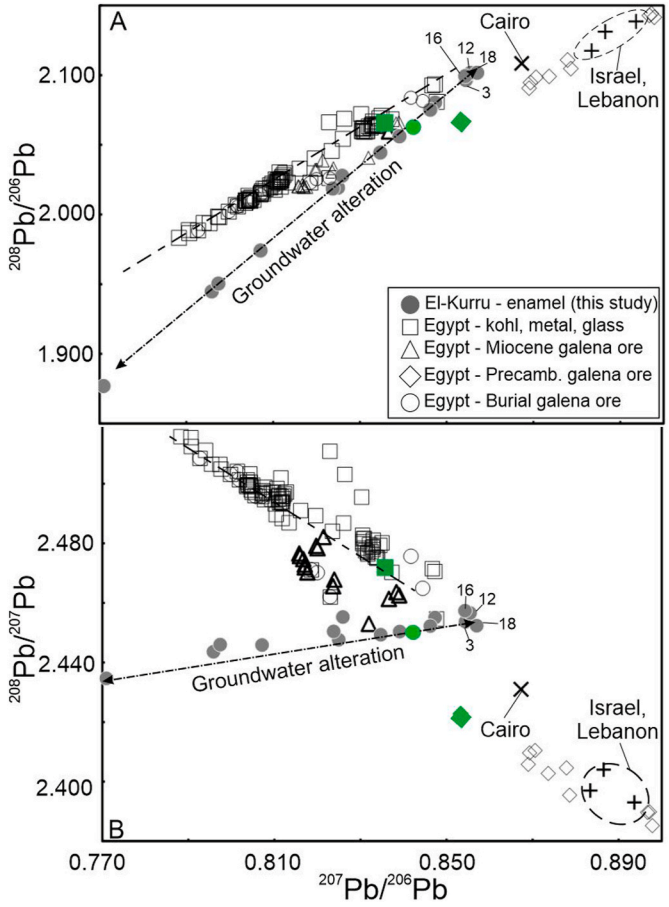

Fig. 7. Plots of $^{207}Pb/^{206}Pb$ versus (A) $^{208}Pb/^{206}Pb$ and (B) $^{208}Pb/^{207}Pb$ for samples of tooth enamel from El-Kurru examined here (solid gray circles). These are compared to the Pb isotope compositions for a variety of archaeological samples (lead ores, kohls, lead metal, copper alloys, glass, glaze and pigment) within Egypt (Stós-Gale and Gale, 1981; Hassan and Hassan, 1981; Shortland et al., 2006), and those modern-day atmospheric aerosols (**X** = Cairo; + = Israel, Lebanon) sampled within the Middle Eastern region (Bollhofer and Rossman, 2000). Solid green square represents the present-day (0 million years, Ma) Pb isotope composition of average continental crust (Stacey and Kramers, 1975). Solid green circle and diamond = average Pb isotope compositions of Neoproterozoic metamorphic rocks from SMC and ANS (shown in Fig. 5), respectively; both are calculated using data from Evuk et al. (2017). Of note, the Pb isotope compositions for sample KUR-4, which are significantly more radiogenic signatures (Table 3), are not illustrated for scaling purposes. Abbreviation Precamb. = Precambrian period (older than 541 million years) and Miocene epoch = 23.03 to 5.3 million years ago. Associated uncertainties are within the size of the symbol. (For interpretation of the references to color in this figure legend, the reader is referred to the Web version of this article.)

contents should ideally be restricted between 100 and 250 ppm for non-diagenetically altered samples (e.g., Dudás et al., 2016). Moreover, the C/MTC values for Sr for the enamel samples studied here are all <1 (Fig. 3), which indicates that Sr abundances have not been impacted by groundwater alteration. Overall, a majority of the enamel samples from El-Kurru plot within this range of Sr abundances (100–250 ppm; Fig. 4) and define two groups in relation to their Sr isotope compositions. The group of samples with lower $^{87}Sr/^{86}Sr$ ratios (<0.7072) define a relatively restricted range (~0.7066–~0.7070) and do not correlate with their corresponding Sr contents; whereas the second group with more radiogenic Sr isotope compositions record more variable (~0.7074–~0.7083) ratios and seem to correlate positively with their Sr abundances (Fig. 4). Thus, the bimodal distribution in the Sr isotope results reported here, in particular for enamel samples with Sr abundances between 100 and 250 ppm (as outlined in Fig. 4), can be interpreted to either represent individuals originating from different regions (i.e., local vs. immigrant), or less likely reflect different degrees of diagenetic alteration.

In order to better evaluate the post mortem alteration hypothesis, Fig. 6 illustrates the $^{87}Sr/^{86}Sr$ ratios versus their corresponding U/Pb values for the El-Kurru enamel samples studied here since the latter parameter may be used to evaluate the degree of diagenetic alteration (e.g., Kohn et al., 1999; Trueman et al., 2008; Koenig et al., 2009; Benson et al., 2013; Kohn and Moses, 2013; Willmes et al., 2016; Kamenov et al., 2018). The group of enamel samples characterized by the lower Sr isotope compositions record a larger range of U/Pb ratios (~0–~1.5) compared to those for the radiogenic (higher) group of enamel samples (~0–~0.3; except for sample KUR-1), with the latter defining a positive trend (Fig. 6a). Moreover, the U/Pb values are in general positively correlated with their Pb isotope compositions (Fig. 6b), which indicate that these record the addition of radiogenic in-growth of Pb originating from the time-integrated decay of U. On the basis of solely the U/Pb ratios reported here, it is difficult to discern exactly which enamel samples record non-diagenetically altered $^{87}Sr/^{86}Sr$ ratios since both groups exhibit trends that may be attributed to the addition of U post-mortem (Fig. 6).

An alternative approach is to compare the Pb isotope ratios for the enamel samples reported here to those for pertinent atmospheric, geological, and anthropogenic (i.e., exposure to extracted Pb ores for human purposes; e.g., pottery glazes, kohls) samples reported within the

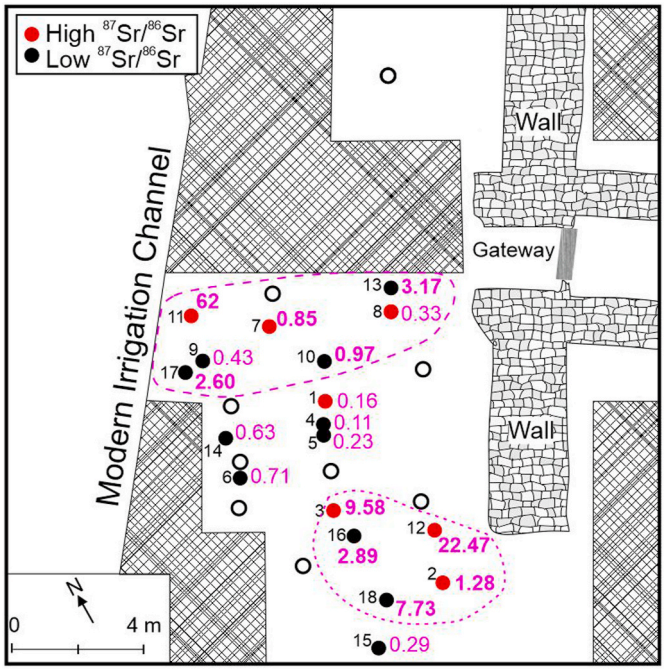

Fig. 8. Plan of the Medieval cemetery at El-Kurru archaeological site showing its position relative to the modern irrigation channel, the brick wall gateway, and later mud-brick domestic architecture adjacent to it (after Dann et al., 2016). The numbers adjacent to red and black solid circles (based on Sr isotope compositions), which indicate position of skeletal remains within cemetery, correspond to sample numbers (Tables 1–3). Also shown are their Pb contents (ppm, purple text). Empty circles represent locations of skeletal remains not investigated here. (For interpretation of the references to color in this figure legend, the reader is referred to the Web version of this article.)

region of the Nile River Valley. Given the unique geochemical nature of the U–Pb radiogenic isotope system, Pb–Pb isotope plots (e.g., Fig. 7) are an effective tool in assessing open-system behavior or mixing of Pb from multiple sources. If a suite of samples has indeed been affected by either of the latter processes, then the result is that the Pb isotope data will be define linear arrays and plot between the two end-member compositions. In Fig. 7, the Pb isotope compositions for the enamel samples from El-Kurru define well-constrained linear arrays with enamel sample KUR-4 recording the most distinct and elevated Pb isotope ratios (Table 3). The results reported here from El-Kurru are compared to those from the studies of Stós-Gale and Gale (1981), Hassan and Hassan (1981), and Shortland (2006), which examined the compositions for a variety of archaeological samples (lead ores, kohls, lead metal, copper alloys, glass, glaze and pigment) within Egypt, which also define a well-constrained linear array (Fig. 7), but with a completely different slope. Both plots in Fig. 7 clearly indicate that the linear arrays defined by the El-Kurru samples are unique when compared to existing data for various environmental and anthropogenic samples within the Nile River Valley. The two linear arrays appear to converge at higher $^{207}Pb/^{206}Pb$ ratios (Fig. 7). Also shown in Fig. 7 are the Pb isotope compositions for modern-day atmospheric aerosols sampled within the Middle Eastern region (Bollhofer and Rossman, 2000); these plot at much higher $^{207}Pb/^{206}Pb$ ratios and do not appear to involve the same end-member (natural and anthropogenic) components as those required to explain the data from either El-Kurru, or other archaeological samples from within the Nile River Valley. Fig. 7 also displays the Pb isotope composition of present-day, average continental crust (Stacey and Kramers, 1975) and the average signatures for Neoproterozoic metamorphic rocks belonging to the SMC and more juvenile samples from the ANS (from Evuk et al., 2017; shown in Fig. 5); these data also plot close to the point of convergence for the Pb–Pb mixing arrays defined by the El-Kurru and Egyptian archaeological samples. Therefore, we postulate that Pb derived from regional bedrock (crust) is one end-member of the El-Kurru mixing line. The second end-member for the El-Kurru requires a component that is U-rich or characterized by a high U/Pb ratio.

Lead present in natural samples that have not been impacted by the addition of U subsequent their time of formation are characterized by Pb isotope compositions that are a function of their age (and their original U/Pb ratio) and these define a relatively restricted range in nature (e.g., $^{207}Pb/^{206}Pb$: ~0.83 to ~1.1 for samples between 0 and 3,000 million years old). In contrast, Pb present in natural samples that was derived solely from radiogenic sources, i.e., it is the result of U decay with no other Pb present at the time of formation is also age dependent and will be characterized by much lower Pb isotope ratios (e.g., $^{207}Pb/^{206}Pb$: ~0.04 to ~0.4). For example, as stated earlier, the best fit linear regression in Fig. 4a defined by the tooth enamel samples from El-Kurru has a slope ~0.0629, which corresponds to Neoproterozoic $^{207}Pb/^{206}Pb$ secondary isochron age. Hence, a sample containing a mixture of natural (geogenic) Pb from its initial time of formation and possibly radiogenic Pb accumulating from a U-rich endmember will record a mixed Pb isotopic signature. Therefore, the Pb–Pb isotope arrays defined by the enamel samples from El-Kurru (Fig. 7) most likely represent mixing between background, crustal Pb and radiogenic Pb accumulated from U-bearing groundwater. Typically, dissolved U is found in most surface water and groundwater at very low concentrations (ppb or ng g^{-1} range), and at much higher values when associated with highly mineralized, thermal and brine waters (Kumar et al., 2011). During bedrock and soil interaction with groundwater, radionuclides may transfer by dissolution, desorption, and erosion (Vongunten and Benes, 1995). The transport of U and other radionuclides in groundwater is dependent on the presence of fractures or faults and their interconnectivity within the bedrock. Moreover, the transport (movement) of U within groundwater depends on multiple factors including diffusion, emanation, and permeability of the rocks (Lopez et al., 2002). The combined elevated abundances of Fe, Nd and U for all the El-Kurru enamel samples as shown by corresponding C/MTC values (Fig. 3) are consistent with post mortem diagenetic alteration (Kamenov et al., 2018). The source of U and the radiogenic Pb incorporated into the samples of tooth enamel most likely emanates from the surrounding Neoproterozoic sandstones and mudstones, which are most likely characterized by U contents of 1–10 ppm (i.e., average continental crust; Rudnick and Gao, 2014). Thus, given the radiogenic nature of the Pb isotope compositions for several enamel samples (KUR-1, -4, -15; Table 2 and Figs. 5–7), the post mortem diagenetic alteration occurred in the recent past so as to provide time to accrue radiogenic Pb from the radioactive decay of U.

Given the elemental abundances and Pb isotope compositions reported here (Tables 2 and 3; Figs. 2–7), tooth enamel samples KUR-3, -12, −16, and −18 contain relatively similar Pb isotope compositions and plot closest to the natural Pb endmember component (Fig. 7); these samples also record elevated contents of Pb (between ~3 and ~23 ppm) and higher corresponding EFs (relative to the remaining samples; Table 2), which suggest these samples have been significantly impacted by groundwater diagenetic alteration. In general, the Pb isotope compositions for most samples correlate with their corresponding U/Pb values (Fig. 6b), and therefore, the Pb–Pb isotope arrays defined by the El-Kurru enamel samples and illustrated in Fig. 7 are interpreted to represent diagenetic alteration by groundwater with variable U/Pb ratios. Of particular importance, these 4 enamel samples (KUR-3, -12, −16, and −18) belong to both groups of Sr isotope compositions (Fig. 4), and their Pb concentrations don't correlate with their corresponding $^{87}Sr/^{86}Sr$ ratios; for example, samples KUR-1, -2, and -11 record similar, higher $^{87}Sr/^{86}Sr$ ratios (range from 0.70748 to 0.70772; Fig. 4; Table 2) but contain extremely variable Pb contents of 0.16, 1.28 and 61.95 ppm (Table 2), respectively. Moreover, Pb contents and Sr isotope compositions of tooth enamel reported here are not a function of their location within the burial site. Fig. 8 illustrates the locations of the skeletal remains at the El-Kurru burial site for the individuals investigated here,

and the enamel samples with the highest Pb concentrations and least radiogenic Pb isotope compositions appear to be concentrated into 2 areas. Within these areas, enamel samples are characterized by a wide range of $^{87}Sr/^{86}Sr$ ratios (from both groups; Fig. 8), and therefore, this feature may be explained in two ways. The first being that the Sr isotope compositions do indeed reflect differing provenance and their $^{87}Sr/^{86}Sr$ ratios were buffered, or not affected by diagenetic alteration because of the much higher contents of Sr in tooth enamel versus that found in groundwater. The fact that there is no correlation between the Sr and Pb isotope compositions (or between Pb contents and Sr isotope ratios) for the tooth enamel samples investigated here lends support to this interpretation. An alternative explanation is that the groundwater entering the shallow burial pits was characterized by variable Sr isotopic compositions, which reflects the Sr isotopic heterogeneity ($^{87}Sr/^{86}Sr$ ratios range between ~0.7032 and ~0.7089) for the surrounding Neoproterozoic basement rocks; these consist of a variety of metamorphic rocks (metagabbro, amphibole schist, granulitic amphibolite) within the surrounding Saharan Metacraton (Evuk et al., 2017). However, there is only an approximate maximum difference of 1.25 m in burial depth elevations for the individuals investigated here (Table 1); therefore, it seems unlikely that the varying Sr isotope compositions reflect a variable hydrological regime that is controlled by the local bedrock geology since the host Cretaceous mudstones, siltstone, and sandstone units are in general of greater thickness than the variation in burial depth (Dann et al., 2016). Moreover, there are no correlations exhibited (not shown) between burial depth elevation of the individuals examined here (Table 1) and any elemental (Table 2) or isotope signatures (Table 3). Thus, our preferred interpretation is that the variable Sr isotope compositions for samples with restricted Sr contents (100–250 ppm; Fig. 4) represent original and non-diagenetically altered signatures that reflect individuals originating from different areas within this region of Sudan.

6. Conclusions

Based on the trace elemental abundances and Sr and Pb isotope results reported in this study, the main conclusions and interpretations are as follows:

- The elevated trace element concentrations, in particular for those of Pb and U, cannot be attributed to human/anthropogenic activities as evidenced by the low EFs (<10) and corresponding Pb isotope compositions. Hence, it is important to note that the Pb isotope results for the tooth enamel samples from El-Kurru are critical in establishing that the extremely radiogenic (high) ratios originate from natural (geogenic) sources;
- The Pb isotope compositions and accompanying Fe, Nd, U and Pb contents (U/Pb ratios) indicate that the Christian-age skeletal remains and samples of tooth enamel from El-Kurru have been impacted by recent groundwater alteration due to the burial site's proximal location to several wadis that have rendered it prone to flooding events in the past;
- Based on the combined trace element results and Pb and Sr isotope compositions reported here, it is most likely that several individuals (e.g., KUR-1, -2, -8, and -11 *vs.* those characterized by lower Sr isotope ratios; Fig. 4) present within the Christian burial site originated from different geographic regions of Sudan. Assessment of their exact geographic origins are beyond the scope of this present study and will be the focus of future investigation.

Declaration of competing interest

The authors declare that they have no known competing financial interests or personal relationships that could have appeared to influence the work reported in this paper.

Acknowledgements

This work was funded by the National Science Foundation (BCS grant #1916718) to A. Simonetti and M.R. Buzon. We thank two anonymous reviewers for their comments and valuable input on an earlier version of the manuscript.

References

Abdel-Rahman, E.M., 1993. Geochemical and geotectonic controls of the metallogenic evolution of selected ophiolite complexes from the Sudan. Berl. Geowiss. Abh. Reihe A 145, 175.
Abdelsalam, M.G., Stern, R.J., Copeland, P., Elfaki, E., Elhur, B., Ibrahim, F.M., 1998. The Neoproterozoic Keraf suture in NE Sudan: sinistral transpression along the eastern margin of west Gondwana. J. Geol. 106, 133–148.
Andrushko, V.A., Buzon, M.R., Simonetti, A., Creaser, R.A., 2009. Strontium isotope evidence for prehistoric migration at Chokepukio, Valley of Cuzco, Peru. Lat. Am. Antiq. 20, 57–75.
Baker, J.A., Peat, D., Waight, T., Meyzen, C., 2004. Pb isotopic analysis of standards and samples using a ^{207}Pb–^{204}Pb double spike and thallium to correct for mass bias with a double-focusing MC-ICP-MS. Chem. Geol. 211, 275–303.
Balboni, E., Jones, N., Spano, T., Simonetti, A., Burns, P.C., 2016. Chemical and Sr isotopic characterization of North America uranium ores: nuclear forensic applications. Appl. Geochem. 74, 24–32.
Bataille, C.P., von Holstein, I.C.C., Willmes, J.E., Liu, X.-M., Davies, G.R., 2018. A bioavailable strontium isoscape for Western Europe: a machine learning approach. PloS One 13, e0197386. https://doi.org/10.1371/journal.pone.0197386.
Benson, A., Kinsley, L., Willmes, M., Defleur, A., Kokkonen, H., Mussi, M., Grün, R., 2013. Laser ablation depth profiling of U-series and Sr isotopes in human fossils. J. Archaeol. Sci. 40, 2991–3000.
Bentley, A.R., 2006. Strontium isotopes from the earth to the archaeological skeleton: a review. J. Archaeol. Method Theor 13, 135–187.
Bercovitz, K., Laufer, D., 1990. Tooth type as indicator of exposure to lead of adults and children. Arch. Oral Biol. 35, 895–897.
Bollhöfer, A., Rosman, K.J.R., 2000. Isotopic source signatures for atmospheric lead: the Southern Hemisphere. Geochem. Cosmochim. Acta 64, 3251–3262.
Bowen, W.H., 2001. Exposure to metal ions and susceptibility to dental caries. J. Dent. Educ. 65, 1046–1053.
Brill, R.H., Wampler, J.M., 1967. Isotope studies of ancient lead. Am. J. Archaeol. 71, 63–77.
Buzon, M.R., Conlee, C.A., Simonetti, A., Bowen, G.J., 2012. The consequences of Wari contact in the Nasca region during the Middle Horizon: archaeological, skeletal, and isotopic evidence. J. Archaeol. Sci. 39, 2627–2636.
Buzon, M.R., Simonetti, A., 2013. Strontium isotope ($^{87}Sr/^{86}Sr$) variability in the Nile Valley: identifying residential mobility during ancient Egyptian and Nubian sociopolitical changes in the new kingdom and Napatan periods. Am. J. Phys. Anthropol. 151, 1–9.
Buzon, M.R., Simonetti, A., Creaser, R.A., 2007. Migration in the Nile Valley during the New Kingdom period: a preliminary strontium isotope study. J. Archaeol. Sci. 34, 1391–1401.
Buzon, M.R., Stuart, T.S., Simonetti, A., 2016. Entanglement and the formation of the ancient Nubian Napatan state. Am. Anthropol. 118, 284–300.
Chenery, C., Müldner, G., Evans, J., Eckardt, H., Lewis, M., 2010. Strontium and stable isotope evidence for diet and mobility in Roman Gloucester, UK. J. Archaeol. Sci. 37, 150–163.
Dann, R.J., Emberling, G., Stearns, C., Antis, S., Skuldbol, T., Uildriks, M., Rose, K., Phillips, J., Breidenstein, A., Miller, N.F., 2016. El Kurru 2015-16 Preliminary Report. Sudan and Nubia, 20, pp. 35–49.
Duce, R.A., Hoffman, G.L., Ray, B.J., Fletcher, I.S., Fletcher, W.G.T., Fasching, J.L., Piotrowicz, S.R., Walsh, P.R., Hoffman, E.J., Miller, J.M., Heffter, J.L., 1976. Trace metals in the marine atmosphere: sources and fluxes. In: Windom, H.L., Duce, R.A. (Eds.), Marine Pollution Transfer. Lexington Books, Blue Ridge Summit, pp. 77–119.
Dudás, F.Ö., LeBlanc, S.A., Carter, S.W., Bowring, S.A., 2016. Pb and Sr concentrations and isotopic compositions in prehistoric North American teeth: a methodological study. Chem. Geol. 429, 21–32.
Emberling, G., Dann, R.J., Abdelwahab Mohamed-Ali, M., Skuldbøl, T., Boaz, B., Cheng, J., Blinkhorn, E., 2013. New Excavations at El Kurru: Beyond the Napatan Royal Cemetery. Sudan and Nubia, 17, pp. 42–60.
Emberling, G., Dann, R.J., Mohamed-Ali, A.S., et al., 2015. A Royal Cemetery of Kush: Archaeological Investigations at El Kurru, Northern Sudan, 2014-15. Sudan and Nubia, 19, pp. 54–70.
Ericson, J.E., 1985. Strontium isotope characterization in the study of prehistoric human ecology. J. Hum. Evol. 14, 503–514.
Evans, J.A., Chenery, C.A., Montgomery, J., 2012. A summary of strontium and oxygen isotope variation in archaeological human tooth enamel excavated from Britain. J. Anal. At. Spectrom. 27, 754–764.
Evans, J., Stoodley, N., Chenery, C., 2006. A strontium and oxygen isotope assessment of a possible fourth century immigrant population in a Hampshire cemetery, southern England. J. Archaeol. Sci. 33, 265–272.
Evuk, D., Lucassen, F., Franz, G., 2017. Lead isotope evolution across the Neoproterozoic boundary between craton and juvenile crust, Bayuda Desert, Sudan. J. Afr. Earth Sci. 135, 72–81.

Faure, G., Mensing, T.M., 2005. Isotopes: Principles and Applications, third ed. John Wiley and Sons, Inc., Hoboken, New Jersey.
Geological Research Authority of the Sudan, 1988. Geologic Map of Sudan. Ministry of Energy & Mines, Geological & Mineral Resources Department, Khartoum.
Gulson, B.L., 1996. Tooth analyses of sources and intensity of lead exposure in children. Environ. Health Perspect. 104, 306–312.
Hassan, A.A., Hassan, F.A., 1981. Source of galena in predynastic Egypt at Nagada. Archaeometry 23, 77–82.
Hoppe, K.A., Koch, P.L., Furutani, T.T., 2003. Assessing the preservation of biogenic strontium in fossil bones and tooth enamel. Int. J. Osteoarchaeol. 13, 20–28.
Iñañez, J.G., Bellucci, J.J., Rodríguez-Alegría, E., Ash, R., McDonough, W., Speakman, R. J., 2010. Romita pottery revisited: a reassessment of the provenance of ceramics from Colonial Mexico by LA-MC-ICP-MS. J. Archaeol. Sci. 37, 2698–2704.
Jenner, G.A., Longerich, H.P., Jackson, S.E., Fryer, B.J., 1990. ICP-MS - a powerful tool for high-precision trace-element analysis in Earth sciences: evidence from analysis of selected U.S.G.S. reference samples. Chem. Geol. 83, 133–148.
Johnston, J.E., Franklin, M., Roh, H., Austin, C., Arora, M., 2019. Lead and arsenic in shed deciduous teeth of children living near a lead-acid battery smelter. Environ. Sci. Technol. 53, 6000–6006.
Kamenov, G.D., Lofaro, E.M., Goad, G., Krigbaum, J., 2018. Trace elements in modern and archaeological human teeth: implications for human metal exposure and enamel diagenetic changes. J. Archaeol. Sci. 99, 27–34.
Knudson, K.J., 2008. Tiwanaku influence in the south central Andes: strontium isotope analysis and Middle horizon migration. Lat. Am. Antiq. 19, 3–23.
Koeman, E.C., Simonetti, A., Burns, P.C., 2015. Sourcing of copper and lead within red inclusions from trinitite postdetonation material. Anal. Chem. 87, 5380–5386.
Koenig, E., Rogers, R.R., Trueman, C.N., 2009. Visualizing fossilization using laser ablation–inductively coupled plasma–mass spectrometry maps of trace elements in late cretaceous bones. Geology 37, 511–515.
Kohn, M.J., Moses, R.J., 2013. Trace element diffusivities in bone rule out simple diffusive uptake during fossilization but explain in vivo uptake and release. Proc. Natl. Acad. Sci. U.S.A. 110, 419–424.
Kohn, M.J., Schoeninger, M.J., Barker, W.W., 1999. Altered states: effects of diagenesis on fossil tooth chemistry. Geochem. Cosmochim. Acta 63, 2737–2747.
Kumar, A., Rout, S., Narayanan, U., Mishra, M.K., Tripathi, R.M., Singh, J., Kumar, S., Kushwaha, H.S., 2011. Geochemical modelling of uranium speciation in the subsurface aquatic environment of Punjab State in India. J. Geol. Min. Res. 3, 137–146.
Küster, D., Liégeois, J.P., 2001. Sr, Nd isotopes and geochemistry of the Bayuda Desert high-grade metamorphic-basement (Sudan): an early Pan-African oceanic convergent margin, not the edge of the East Saharan ghost craton. Precambrian Res. 109, 1–23.
Kyle, J.H., 1986. Effect of post-burial contamination on the concentrations of major and minor elements in human bones and teeth – the implications for palaeodietary Research. J. Archaeol. Sci. 13, 403–416.
Lee-Thorp, J., Sponheimer, M., 2003. Three case studies used to reassess the reliability of fossil bone and enamel isotope signals for paleodietary studies. J. Anthropol. Archaeol. 22, 208–216.
LeGeros, R., 1991. Calcium phosphates in enamel, dentine and bone. In: Myres, H. (Ed.), Calcium Phosphates in Oral Biology, fifteenth ed. Karger, Basel, pp. 108–129.
Lopez, R.N., Segovia, N., Cisiega, M.G., Lopez, M.B.E., Armienta, M.A., Seidel, J.L., Pena, P., Godinez, L., Tamez, E., 2002. Determination of radon, major and trace elements in water samples from springs and wells of northern Mexico State, Mexico. Geofisc. Int. 41, 407–414.
Manhes, G., Allègre, C.J., Dupré, B., Hamelin, B., 1980. Lead isotope study of basic ultrabasic layered complexes: speculations about the age of the Earth and primitive mantle characteristics. Earth Planet Sci. Lett. 47, 370–382.
Maurer, A.F., Person, A., Tütken, T., Amblard-Pison, S., Ségalen, L., 2014. Bone diagenesis in arid environments: an intraskeletal approach. Palaeogeogr. Palaeoclimatol. Palaeoecol. 416, 17–29.
Mirnejad, H., Simonetti, A., Molasalehi, F., 2011. Pb isotopic compositions of some Zn–Pb deposits and occurrences from Urumieh–Dokhtar and Sanandaj–Sirjan zones in Iran. Ore Geol. Rev. 39, 181–187.
Mirnejad, H., Simonetti, A., Molasalehi, F., 2015. Origin and formational history of some Pb-Zn deposits from Alborz and Central Iran: Pb isotope constraints. Int. Geol. Rev. 57, 463–471.
Montgomery, J., 2002. Lead and Strontium Isotope Compositions of Human Dental Tissues as an Indicator of Ancient Exposure and Population Dynamics. PhD, University of Bradford, UK, p. 382. https://doi.org/10.5284/1000249.
Montgomery, J., 2010. Passports from the past: investigating human dispersals using strontium isotope analysis of tooth enamel. Ann. Hum. Biol. 37, 325–346.
Nelson, B.K., Deniro, M.J., Schoeninger, M.J., DePaolo, D.J., Hare, P.E., 1986. Effects of diagenesis on strontium, carbon, nitrogen, and oxygen concentration and isotopic concentration of bone. Geochem. Cosmochim. Acta 50, 1941–1949.
Nielsen-Marsh, C.M., Hedges, R.E.M., 2000. Patterns of diagenesis in bone I: the effects of site environments. J. Archaeol. Sci. 27, 1139–1150.
Prohaska, T., Latkoczy, C., Schultheis, G., Teschler-Nicola, M., Stingeder, G., 2002. Investigation of Sr isotope ratios in prehistoric human bones and teeth using laser ablation ICPMS and ICP-MS after Rb/Sr separation. J. Anal. At. Spectrom. 17, 887–891.
Purchase, N.G., Fergusson, J.E., 1986. Lead in teeth: the influence of the tooth type and the sample within a tooth on lead levels. Sci. Total Environ. 52, 239–250.
Retzmann, A., Budka, J., Sattmann, H., Irrgeher, J., Prohaska, T., 2019. The New kingdom population on Sai Island: application of Sr isotopes to investigate cultural entanglement in Ancient Nubia. In: Ägypten und Levante/Egypt and the Levant, 29, pp. 355–380.
Rudnick, R.L., Fountain, D.M., 1995. Nature and composition of the continental crust: a lower crustal perspective. Rev. Geophys. 33, 267–309.
Rudnick, R.L., Gao, S., 2014. Composition of the continental crust. In: Treatise on Geochemistry (2nd Edition). Reference Module in Earth Systems and Environmental Sciences, vol. 4, pp. 1–51.
Samuelsen, J.R., Potra, A., 2020. Biologically available Pb: a method for ancient human sourcing using Pb isotopes from prehistoric animal tooth enamel. J. Archaeol. Sci. 115, 105079. https://doi.org/10.1016/j.jas.2020.105079.
Sangster, D.F., Outridge, P.M., Davis, W.J., 2000. Stable lead isotope characteristics of lead ore deposits of environmental significance. Environ. Rev. 8, 115–147.
Schrader, S.A., Buzon, M.R., Corcoran, L., Simonetti, A., 2019. Intraregional $^{87}Sr/^{86}Sr$ variation in Nubia: new insights from the third cataract. J. Archaeol. Sci.: For. Rep. 24, 373–379.
Schurr, M.R., Donohue, P.H., Simonetti, A., Dawson, E.L., 2018. Multi-element and lead isotope characterization of early nineteenth century pottery sherds from Native American and Euro-American sites. J. Archaeol. Science: For. Rep. 20, 390–399.
Schweissing, M.M., Grupe, G., 2003. Stable strontium isotopes in human teeth and bone: a key to migration events of the late Roman period in Bavaria. J. Archaeol. Sci. 30, 1373–1383.
Shortland, A.J., 2006. Application of lead isotope analysis to a wide range of Late Bronze age Egyptian Materials. Archaeometry 48, 657–669.
Sillen, A., 1986. Biogenic and diagenetic Sr/Ca in plio-pleistocene fossils of the omo shungura formation. Paleobiology 12, 311–323.
Simonetti, A., Gariepy, C., Banic, C., Tanabe, R., Wong, H., 2004. Pb isotopic investigation of aircraft-sampled emissions from the Horne smelter (Rouyn, Quebec): implications for atmospheric pollution in northeastern North America. Geochem. Cosmochim. Acta 68, 3285–3294.
Simons, T.J., 1986. Cellular interactions between lead and calcium. Br. Med. Bull. 42, 431–434.
Simpson, R., Cooper, D.M.L., Swanston, T., Coulthard, I., Varney, T.L., 2021. Historical overview and new directions in bioarchaeological trace element analysis: a review. Archaeol. Anthropol. Sci. 13 (1), 24. https://doi.org/10.1007/s12520-020-01262-4.
Slovak, N.M., Paytan, A., 2012. Applications of Sr isotopes in archaeology, 743–768. In: Baskaran, M. (Ed.), Handbook of Environmental Isotope Geochemistry, vol. I (Berlin, Heidelberg).
Slovak, N.M., Paytan, A., Wiegand, B.A., 2009. Reconstructing Middle Horizon mobility patterns on the coast of Peru through strontium isotope analysis. J. Archaeol. Sci. 36, 157–165.
Sponheimer, M., Lee-Thorp, J.A., 2006. Enamel diagenesis at South African Australopith sites: implications for paleoecological reconstruction with trace elements. Geochem. Cosmochim. Acta 70, 1644–1654.
Stacey, J.S., Kramers, J.D., 1975. Approximation of terrestrial lead isotope evolution by a two-stage model. Earth Planet Sci. Lett. 26, 207–222.
Steele, D.G., Bramblett, C.A., 1988. The Anatomy and Biology of the Human Skeleton. Texas A&M University, College Station, TX.
Stós-Gale, Z.A., Gale, N.H., 1981. Sources of Galena, lead and silver in predynastic Egypt. In: Revue d'Archéométrie, n°1, 1981. Actes du XXe symposium international d'archéométrie, Paris 26-29 mars 1980, vol. III, pp. 285–296.
Szostek, K., Mądrzyk, K., Cienkosz-Stepańczak, B., 2015. Strontium isotopes as an indicator of human migration– easy questions, difficult answers. Anthropol. Rev. 78, 133–156.
Trueman, C.N., Palmer, M.R., Field, J., Privat, K., Ludgate, N., Chavagnac, V., Eberth, D. A., Cifelli, R., Rogers, R.R., 2008. Comparing rates of recrystallisation and the potential for preservation of biomolecules from the distribution of trace elements in fossil bones. C. R. Palevol. 7, 145–158.
Turner, B.L., Kamenov, G.D., Kingston, J.D., Armelagos, G.J., 2009. Insights into immigration and social class at Machu Picchu, Peru based on oxygen, strontium, and lead isotopic analysis. J. Archaeol. Sci. 36, 317–332.
Vongunten, H.R., Benes, P., 1995. Speciation of radionuclides in the environment. Radiochim. Acta 69, 1–29.
Welsby, D.A., 2002. The Medieval Kingdoms of Nubia: Pagans, Christians and Muslims along the Middle Nile. British Museum Press, London.
Willmes, M., Kinsley, L., Moncel, M.H., Armstrong, R.A., Aubert, M., Eggins, S., Grün, R., 2016. Improvement of laser ablation in situ micro-analysis to identify diagenetic alteration and measure strontium isotope ratios in fossil human teeth. J. Archaeol. Sci. 70, 102–116.
Wychowanski, P., Malkiewicz, K., 2017. Evaluation of metal ion concentration in hard tissues of teeth in residents of Central Poland. BioMed Res. Int. 2017, 6419709. https://doi.org/10.1155/2017/6419709.